I&EC research
Industrial & Engineering Chemistry Research

Article

pubs.acs.org/IECR

Influence of Reaction Atmosphere (H_2O, N_2, H_2, CO_2, CO) on Fluidized-Bed Fast Pyrolysis of Biomass Using Detailed Tar Vapor Chemistry in Computational Fluid Dynamics

Pelle Mellin,*[,†,§] Xi Yu,*[,‡] Weihong Yang,[†] and Wlodzimierz Blasiak[†]

[†]KTH Royal Institute of Technology, Unit of Processes, Brinellvägen 23, 100 44 Stockholm, Sweden
[‡]Aston University, European Bioenergy Research Institute (EBRI), Birmingham B4 7ET, U.K.
[§]Swerea KIMAB AB, Department of Process Development, Isafjordsgatan 28A, 16440 Kista, Sweden

ABSTRACT: Secondary pyrolysis in fluidized bed fast pyrolysis of biomass is the focus of this work. A novel computational fluid dynamics (CFD) model coupled with a comprehensive chemistry scheme (134 species and 4169 reactions, in CHEMKIN format) has been developed to investigate this complex phenomenon. Previous results from a transient three-dimensional model of primary pyrolysis were used for the source terms of primary products in this model. A parametric study of reaction atmospheres (H_2O, N_2, H_2, CO_2, CO) has been performed. For the N_2 and H_2O atmosphere, results of the model compared favorably to experimentally obtained yields after the temperature was adjusted to a value higher than that used in experiments. One notable deviation versus experiments is pyrolytic water yield and yield of higher hydrocarbons. The model suggests a not overly strong impact of the reaction atmosphere. However, both chemical and physical effects were observed. Most notably, effects could be seen on the yield of various compounds, temperature profile throughout the reactor system, residence time, radical concentration, and turbulent intensity. At the investigated temperature (873 K), turbulent intensity appeared to have the strongest influence on liquid yield. With the aid of acceleration techniques, most importantly dimension reduction, chemistry agglomeration, and in-situ tabulation, a converged solution could be obtained within a reasonable time (~30 h). As such, a new potentially useful method has been suggested for numerical analysis of fast pyrolysis.

1. INTRODUCTION

The fast pyrolysis process is promising for production of tar-based fuels and chemicals. However, the complexity of the underlying chemistry is vast and understanding it is challenging to say the least. We aim, however, as a continuation of our previous work[1−3] to model fast pyrolysis with the present means and understanding, utilizing computational fluid dynamics (CFD) to study pyrolysis of biomass inside a reactor. Such an approach has been termed chemical conversion modeling,[4] in contrast to single-particle models.

The starting approach is to simulate primary pyrolysis, which is biomass decomposition controlled by the heat and momentum interaction with the bed material (e.g., sand or catalyst). As such, a model for the multiphase interaction has been devised to estimate the formation rates of primary products, which emerge from the solid biomass particles. This has been done in a fluidized bed with steam and nitrogen as fluidizing agent to see the differences due to the physical properties of the reaction atmosphere.[2] However, once the primary products form a liquid and evaporate from the particle, secondary pyrolysis takes place and we assume the reaction atmosphere will provide both physical and chemical effects.

To date, there are few detailed reports on the effects of atmosphere (H_2O, N_2, H_2, CO_2, and CO) on pyrolysis. Such reactive atmospheres are commonly known to influence yield and quality of products. But it is not known exactly why and how specific properties contribute. By linking these properties through models with the effects that can be seen in experiments, opportunities for optimization can arise. Further understanding of gas recirculation and downstream upgrading of the liquid product can also be gained. The advantage of models in this case is that one specific property can be linked to a certain contribution in the secondary pyrolysis, while many aspects of the whole process are still considered.

1.1. Tar Vapor Composition.

Organic tar mixtures with large molecular weight, or primary tar, are originally formed from solid biomass via primary pyrolysis. Primary tar is formed in the absence of oxygen, in a temperature range of 400−700 °C. With continuous exposure to a heated environment, primary tar can undergo secondary tar reactions (STR), which alter both mass and composition of the resulting liquid.[5] STR, as a term, includes all reactions after primary pyrolysis; however, in the context of such work as Morf et al.,[5] reactions important for gasification are primarily considered. If instead secondary tar reactions are defined according to Milne et al.[6] (see Figure 1), the first secondary reactions start inside the pyrolyzing biomass particle or close, in the vapor phase, at relatively low temperatures. In fact, some studies found the early STR hard to study in a reactor environment because they occur quickly.[7] But describing these reactions in a fast pyrolysis reactor environment could be helpful for understanding the behavior and possible effect of reactor configurations or operating conditions.

Received: June 15, 2015
Revised: July 26, 2015
Accepted: July 29, 2015
Published: July 29, 2015

DOI: 10.1021/acs.iecr.5b02164
Ind. Eng. Chem. Res. 2015, 54, 8344−8355

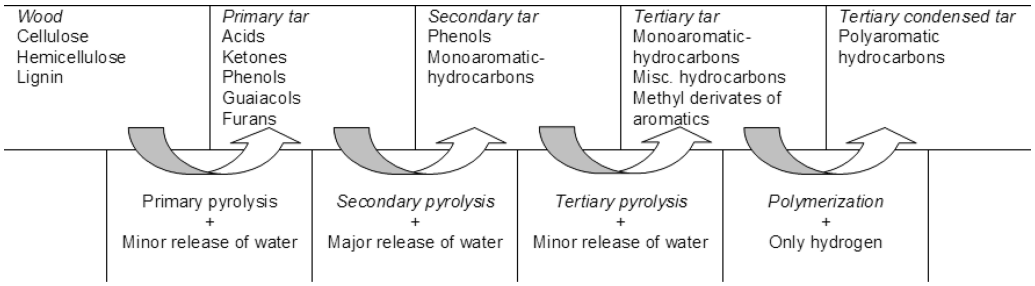

Figure 1. Idea of tar maturation adopted from Milne et al.[6] shown alongside the different pyrolysis stages with amount of formed water (note that the figure is redrawn by the authors, from ref 8).

Tar composition changes, especially via STR, but in CFD models, it is rarely considered. In fact, secondary pyrolysis is normally considered lumped, see eq 1 from refs 9 and 10; as such, the actual composition of the *tar* is disregarded. In that case, the yields of liquid and solid residue as well as the stoichiometric coefficients of noncondensable gases (NCG) in the model are tailored to fit experimental data; for gasification, the reaction represents the cracking of inert tar to syngas, while in fast pyrolysis it represents the liquid yield loss.

$$\text{Tar} \rightarrow \alpha_1\text{CO} + \alpha_2\text{CO}_2 + \alpha_3\text{CH}_4 + \alpha_4\text{H}_2 + \alpha_5\text{Tar}_{\text{inert}} + \alpha_6\text{Char} \quad (1)$$

It is noted that the tar we discuss and study in this work refers to tar vapor during pyrolysis process before being quenched in the scrubber.

1.2. Comprehensive Kinetics. During recent years, comprehensive kinetic models of the secondary pyrolysis have been developed, partly to support combustion models. Models of the formation of soot, polyaromatic hydrocarbons, and other emissions require comprehensive understanding of not only the oxidation of various compounds but also pyrolysis and polymerization.

In this work, the secondary pyrolysis is considered as one step in the commonly accepted tar maturation scheme previously introduced by Milne et al.,[6] see Figure 1. As the tar matures, which is assumed to occur in three stages, the composition changes, with temperature being a prominent factor. To describe this, a number of chemistry schemes have been published recently. For instance, Elfasakhany[11] developed a functional group model for modeling of STR. Ranzi et al.[12] developed a kinetic model which describes the homogeneous gas phase reactions with a high number of species and reactions. Norinaga et al.[13] extended the same model to include additional hydrocarbon chemistry.

STR can be categorized into two classes, homogeneous and heterogeneous. Homogeneous STR has been widely studied.[8−10] The studies on heterogeneous STR—although limited in numbers—commonly found that tar decomposes in presence of biochar. In fact, Zhang et al.[18] concluded that heterogeneous STR contributes more than homogenous STR during naphthalene decomposition. In contrast, Gilbert et al.[14] pointed out that biochar showed no significant increase in cracking of tar and tar removal, which in that work occurred because of homogeneous cracking. During fast pyrolysis, the typical temperature regime (850−1000 °C) which produces of tertiary tar—aromatics in particular, such as naphthalene—is not reached. The difference in used reference compounds for the fast pyrolysis might explain the different results. It highlights the complexity of the chemistry and that different compounds might respond differently. This is a good reason for treating the tar vapor as not one single compound and adopting comprehensive chemistry schemes.

In the attempt to model biomass pyrolysis after primary pyrolysis by simple thermal cracking reaction (see Mellin et al.[2]), it was found that too little pyrolytic water formed because of missing secondary pyrolysis reactions in the model framework (presumed to comprise the major part of pyrolytic water, see the lower part of Figure 1). On the other hand, the reactions helped in obtaining a char yield closer to the measured char yield. But for the NCG and condensable vapors, a comprehensive kinetic model might better predict this critical part for fast pyrolysis.

2. METHODOLOGY

The pilot plant, on which the previous model was based, has been assembled at KTH Royal Institute of Technology in Sweden. The experiments performed in support of the previous work[1−3] used either steam or nitrogen as fluidizing agent. Figure 2 shows the setup with the extent of the model in this work indicated.

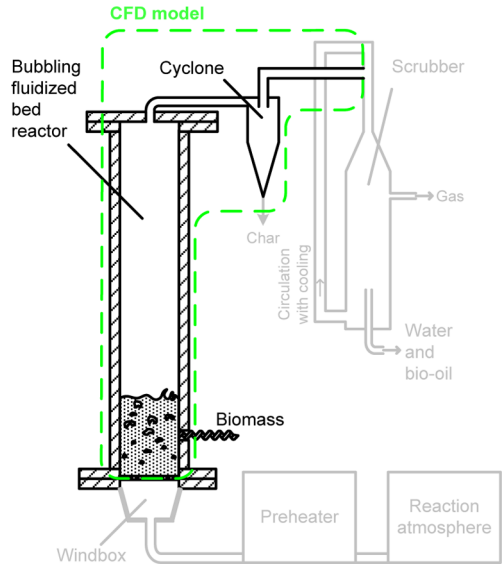

Figure 2. Pilot plant with the extent of the CFD model shown.

As mentioned in the Introduction, the chemical effects are the focus of this work; which is understood as the interaction of steam and other atmospheres with components in the homogeneous gas phase. This paper describes the effort to implement these homogeneous gas phase reactions in a CFD framework and results of simulations close to experimental

DOI: 10.1021/acs.iecr.5b02164
Ind. Eng. Chem. Res. 2015, 54, 8344−8355

Table 1. Species of Tar and Gas in the Kinetic Scheme Implemented in the Composition PDF Model

C no.	suggested name (CHEMKIN scheme designation)				
0	helium^{E} (He)	argon^{E} (Ar)	nitrogen^{E} (N_2)	oxygen^{E} (O_2)	hydrogen peroxide^{E} (H_2O_2)
	water^{E} (H_2O)	hydrogen^{E} (H_2)			
1	graphite^{E} (C)	carbon dioxide^{E} (CO_2)	formic acid^{E} (HCOOH)	formaldehyde^{E} (CH_2O)	performic acid^{E} (HCO_3H)
	carbon monoxide^{E} (CO)				
2	methane^{E} (CH_4)	methanol^{E} (CH_3OH)	acetylene^{E} (C_2H_2)	ketene^{E} (CH_2CO)	glyoxal^{E} ($C_2H_2O_2$)
	ethene^{E} (C_2H_4)	oxirane^{E} (C_2H_4O)	acetaldehyde^{E} (CH_3CHO)	hydroxyacetaldehyde^{E} ($C_2H_4O_2$)	acetic acid^{E} (CH_3COOH)
	ethanol^{E} (C_2H_5OH)	ethane^{E} (C_2H_6)	1,2-ethanediol^{E} (GLIET)	peracetic acid^{E} (CH_3CO_3H)	
3	acrolein^{E} (C_2H_3CHO)	propanedial^{E} ($C_3H_4O_2$)	hydroxyl-oxo-propanal^{E} ($C_3H_4O_3$)	propene^{E} (C_3H_6)	propanal^{E} (C_2H_5CHO)
	acetone^{E} (CH_3COCH_3)	propanal^{E} (C_3H_6O)	acetol^{E} ($C_3H_6O_2$)	propane^{E} (C_3H_8)	propyl-hydroperoxide^{E} (C_3H_7OOH)
	glycerol^{E} (glycerol)	isopropenyl^{E} (CH_2CCH_3)	allene^{E} (*a*-C_3H_4)	propyne^{E} (*p*-C_3H_4)	propanoic acid^{E} (C_3H_5OOH)
4	diacetylene^{E} (C_4H_2)	furan^{E} (C_4H_4O)	butadiene^{E} (C_4H_6)	methacrolein^{E} (*i*-C_3H_5CHO)	isobutene^{E} (*i*-C_4H_8)
	vinylacetylene^{E} (C_4H_4)	*n*-butene^{E} (*n*-C_4H_8)	butadienal^{E} ($CH_2CCHCHO$)	butanedione^{E} ($C_4H_6O_2$)	
> 4	furfural^{E} ($C_5H_4O_2$)	methylfuran^{E} (MEFU2)	cyclopentene^{E} (C_5H_8)	benzene^{E} (C_6H_6)	anhydro-levoglucosan^{E} ($C_6H_8O_4$)
	phenol^{E} (C_6H_5OH)	HMFU^{E} ($C_6H_6O_3$)	methylcyclopentadiene^{E} (MCPTD)	dimethylfuran^{E} (DMF)	benzaldehyde^{E} (C_6H_5CHO)
	xylan^{E} ($C_5H_8O_4$)	cresol^{E} (C_7H_8O)	levoglucosan^{E} ($C_6H_{10}O_5$)	pyrylium^{E} (C_5H_5O)	methoxybenzene^{E} ($C_6H_5OCH_3$)
	syringol^{E} ($C_8H_{10}O_3$)	*p*-coumaryl^{E} ($C_9H_{10}O_2$)	naphthalene^{E} ($C_{10}H_8$)	lumped-phenol^{E} ($C_{11}H_{12}O_4$)	toluene^{E} (C_7H_8)
	p-tolyl^{E} ($C_6H_4CH_3$)	3-cyclopentenyl^{E} (C_5H_7)			

^{E}Exempted from the dimension reduction.

Table 2. Radical Species in the Kinetic Scheme Implemented in the Composition PDF Model

C no.	suggested name (CHEMKIN scheme designation)				
0	oxygen^{R,E} (O)	hydrogen^{R,E} (H)	hydroxyl^{R,E} (OH)	hydroperoxyl^{R,E} (HO_2)	
1	carbyne^{R,E} (CH)	formyl^{R,E} (HCO)	carbene^{R,E} (CH_2)	methyl-peroxy^{R,E} (CH_3OO)	hydroxymethyl^{R,E} (CH_2OH)
	methyl^{R,E} (CH_3)	methoxy^{R,E} (CH_3O)	carbene^{R,E} (CH_2S)	hydroperoxide-methyl^{R,E} (CH_3OOH)	hydrogen carbonate^{R,E} (HCO_3)
2	ethynyl^{R,E} (C_2H)	ketenyl^{R,E} (HCCO)	ethyl-peroxy^{R} (C_2H_5OO)	ketohydroperoxy-ethyl^{R,E} (C_2–OQOOH)	hydroperoxy-Ethylperoxy^{RS} (C_2–OOQOOH)
	ethyl^{R,E} (C_2H_5)	vinoxy^{R,E} (CH_2CHO)	2-hydroxyethyl^{R} (C_2H_4OH)	1-hydroxyethyl^{R} (CH_3CHOH)	ethyl-hydroperoxide^{R,E} (C_2H_5OOH)
	acetyl^{R,E} (CH_3CO)	ethylidyne^{R,E} (C_2H_3)	peroxyacetyl^{R,E} (CH_3CO_3)	hydroperoxy-ethyl^{R} (C_2-QOOH)	
3	allyl^{R} (CH_2CHCH_2)	methylvinoxy^{R} (CH_3COCH_2)	ketohydroperoxy-propyl^{R,E} (C_3–OQOOH)	isoketohydroperoxy-propyl^{R} (*i*-C_3–OQOOH)	*n*-propylperoxy^{R} (*n*-C_3H_7OO)
	propenyl^{R} (*n*-C_3H_7)	cyclopropenyl^{R} (C_3H_3)	propylene-peroxide^{R} (C_3H_5OO)	iso-propyl peroxy^{R} (*i*-C_3H_7OO)	hydroperoxy-propylperoxy^{R} (*n*-C_3–OOQOOH)
	iso-propenyl^{R} (*i*-C_3H_7)	*n*-propoxy^{R} (*n*-C_3H_7O)	hydroperoxy-propyl^{R} (*n*-C_3-QOOH)	cyclopropenylidene^{BR,E} (C_3H_2)	iso-hydroperoxy-propyl^{R} (*i*-C_3-QOOH)
	propanal^{R} (C_2H_4CHO)	propyne^{R} ($CHCHCH_3$)			
4	furanyl^{R} (C_4H_3O)	methylallyl (*s*-C_4H_7)	cyclobutadiene^{R} (C_4H_3)	iso-methylallyl^{R} (*i*-C_4H_7)	methylcyclopropyl^{R} ($CH_2C_3H_5$)
	methylallenyl^{R} (C_4H_5)				
> 4	benzyl^{R} (C_7H_7)	cresol-O^{R} (C_7H_7O)	cresol-C^{R} (C_7H_7O)	cyclopentadienyl^{R} (CYC_5H_5)	dimethylfuranyl^{R} (DMF-3YL)
	phenyl^{R} (C_6H_5)	phenolate^{R} (C_6H_5O)	3-cyclopentenyl^{R} (C_5H_7)	cyclopentadiene^{R,E} (CYC_5H_6)	

^{R}Radical. ^{BR}Biradical. ^{E}Exempted from the dimension reduction.

conditions. A kinetic scheme in CHEMKIN format, comprising 134 species and 4169 reactions (version 1311, available from creckmodeling.chem.polimi.it), was used in the CFD environment of ANSYS Fluent 14.5. The kinetic scheme was introduced by Ranzi et al.[15] and used in Calonaci et al.[16] to study fast pyrolysis at the particle level, with a predetermined residence time for the secondary pyrolysis.

In this work, a residence time of tar vapor (before being quenched in the scrubber) close to the experimental conditions has been achieved by setting up the simulation as described. The implementation of the kinetic scheme was done while at the same time accounting for any turbulence interaction. For the comprehensive chemistry and fluid dynamics, a probability density function (PDF) approach is used. The PDF model, which simulates the flow by a collection of stochastic "fluid particles", has the advantage of avoiding detailed treatment of chemistry and saves computational cost in the combustion simulation of a gas phase. A comprehensive understanding of

DOI: 10.1021/acs.iecr.5b02164
Ind. Eng. Chem. Res. 2015, 54, 8344−8355

the theoretical foundations of the PDF approach can be found in Bope.[17] Wang and Yan[19] mentioned the PDF method as one of the available CFD models for solving turbulent-chemistry interaction.

2.1. Kinetic Model. The chemistry scheme, at 134 species, is reduced to 100 species using a dimension reduction algorithm. The reason is to reach the hard software limit of ANSYS Fluent 14.5. Table 1 gives the species implemented into the CFD model; the exempted compounds from the dimension reduction are indicated with a superscripted *E*. Table 2 shows the radicals in the model which play an important role in most of the reactions in the kinetic scheme.

Figure 3 shows the general outline of the reactions; simple decomposition reactions (first order) occur alongside H-abstraction, oxidation, as well as recombination reactions. The primary compounds that stay unreacted will reach the outlet and be accounted for as part of the mix. New components are also given in Figure 3 which can form only because of secondary pyrolysis. In this paper, no heterogeneous reactions are considered, despite their importance. This is an obvious limitation in the current model, and it should be addressed in future work.

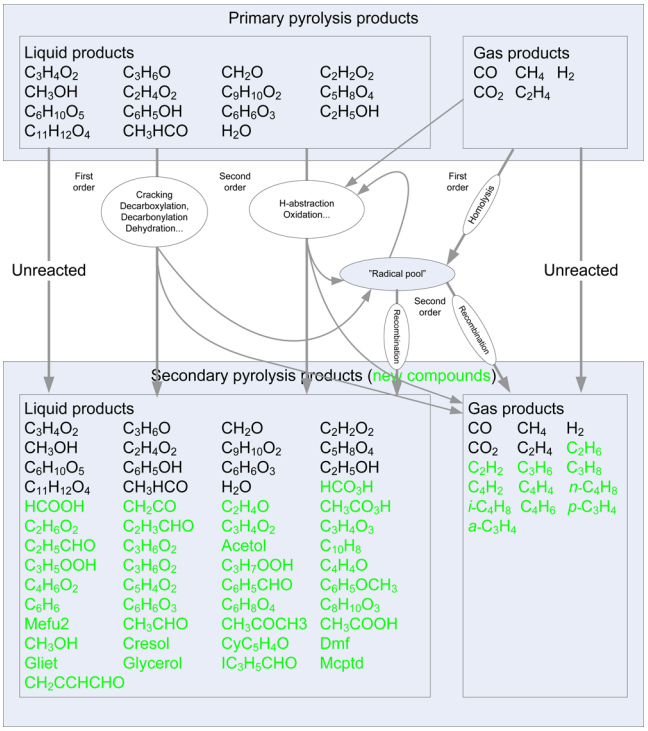

Figure 3. Indicative reactions in the chemistry scheme and new products in addition to the primary products.

2.2. Computational Fluid Dynamics Model. The CFD model coupled with the secondary pyrolysis scheme is developed in ANSYS Fluent v 14.5, using user defined functions (UDF) to describe the source terms (primary product formation) and boundary conditions such as wall temperature and bed zone temperature. More information on the primary pyrolysis model can be found in Mellin et al.[1,2]

The simulation uses a setup based on steady state with a SIMPLE scheme for the pressure−velocity coupling and first-order accuracy for momentum, turbulent kinetic energy, and turbulent dissipation rate. However, by switching to second-order accuracy, no effect on the results could be observed.

2.2.1. Geometry and Mesh. The geometry of the two-dimensional (2-D) model (used in this work) and the three-dimensional (3-D) model (used in previous work) matches so that the formation rate of primary products can be transferred between the models. The mesh in the model for this paper consists of 6565 quadratic cells in a structured 2-D grid. In the previous model, a mesh of 158 998 hexahedral cells was used for the reactor only. The geometry and dimension (the diameter is 0.072 m and the height is 0.95 m) of the fluidized bed is shown in Figure 4.

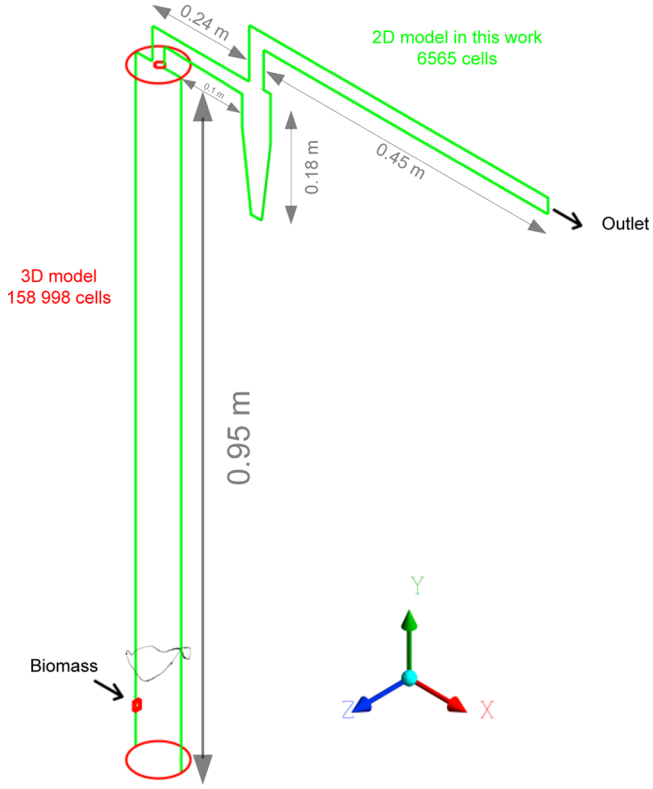

Figure 4. Geometry and overlay of the two combined CFD models. Diameter of the reactor is 7.21 cm.

2.2.2. Chemistry and Turbulence. A steady-state PDF transport simulation was done in a 2-D domain with 20 particles per cell. About 6000 iterations were required for the solution to converge (about 20 000 when using high turbulence at the inlet). Because of the computational load of integrating the chemical source term in eq 3, several acceleration techniques were used. Most importantly, the reaction step in eq 3 was performed by in-situ adaptive tabulation (ISAT).[20] ISAT was employed to dynamically tabulate the chemistry mappings and accelerate the time to solution (accelerations of 2−3 orders of magnitude are typical). Also, chemistry agglomeration in the ANSYS FLUENT 14.5 package was used to cluster cells with similar compositions before they are sent to the ordinary differential equation integrator.

Because of the high turbulence of the flow in the freeboard and cyclone, the standard K-epsilon turbulence and energy dissipation equations proposed by Launder and Spalding[21] were also incorporated in the model, and these are given as follows. Turbulence momentum is described by eq 2, and

DOI: 10.1021/acs.iecr.5b02164
Ind. Eng. Chem. Res. 2015, 54, 8344−8355

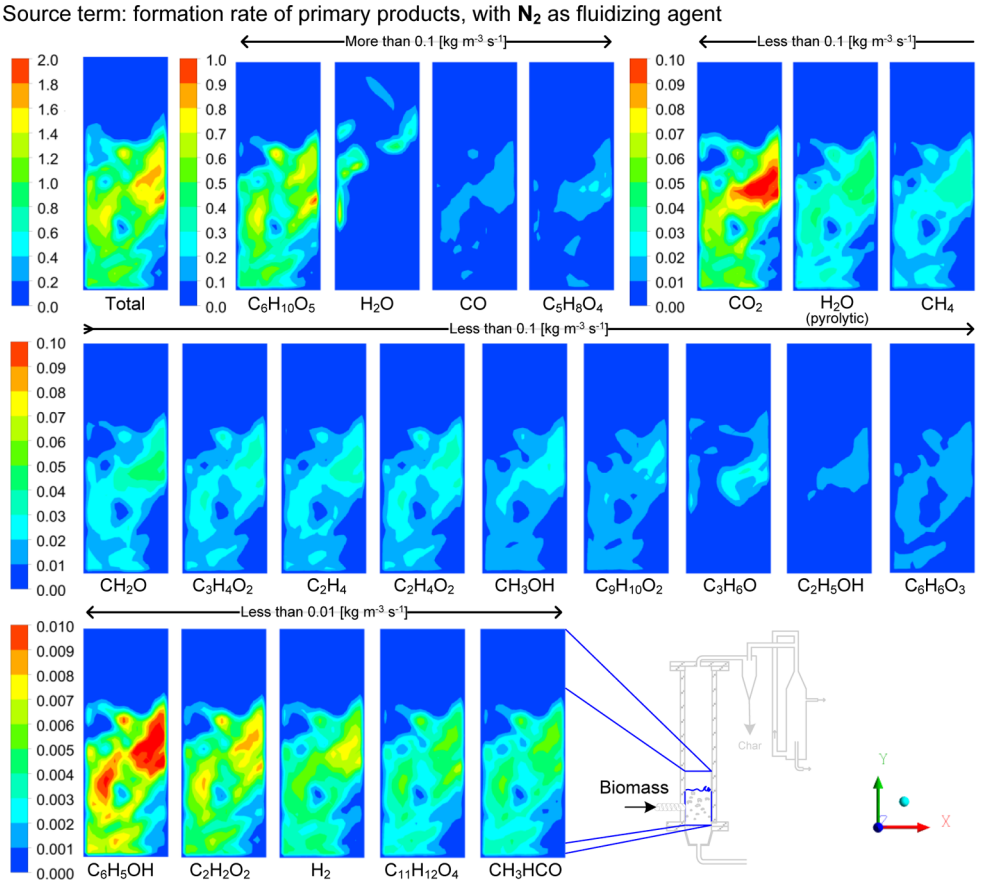

Figure 5. Instantaneous formation rate of individual primary products, implemented from the 3-D results from Mellin et al.,[2] with nitrogen as fluidizing agent. Note that formed H_2O includes evaporated moisture and pyrolytic water (symbolized as H_2O (pyrolytic)).

turbulent kinetic energy dissipation is described by eq 3, where $G_{k,g}$ is described by eq 4 and C_μ by eq 5. C_μ, $C_{1\varepsilon}$, and $C_{2\varepsilon}$ are dimensionless constants; $G_{k,g}$ is the production of turbulent kinetic energy (kg m^{-1} s^{-2}), k_g the turbulent kinetic energy (m^2 s^{-2}), and ε_g the turbulent dissipation rate (m^2 s^{-3}); and $\mu_{l,g}$ and $\mu_{t,g}$ are the viscosities of the gas phase due to laminar and turbulent flow, respectively (Pa s). σ_k and σ_ε are dimensionless constants.

$$\frac{\partial(\alpha_g\rho_g k_g)}{\partial t} + \nabla(\alpha_g\rho_g\vec{u}_g k_g) = \alpha_g G_{k,g} + \nabla\left(\alpha_g\frac{\mu_{t,g}}{\sigma_k}k_g\right) - \alpha_g\rho_g\varepsilon_g \quad (2)$$

$$\frac{\partial(\alpha_g\rho_g\varepsilon_g)}{\partial t} + \nabla(\alpha_g\rho_g\vec{u}_g\varepsilon_g) = \nabla\left(\alpha_g\frac{\mu_{t,g}}{\sigma_\varepsilon}\varepsilon_g\right) + \alpha_g\frac{\varepsilon_g}{k_g}(C_{1\varepsilon}G_{k,g} - C_{2\varepsilon}\rho_g\varepsilon_g) \quad (3)$$

$$G_{k,g} = \mu_{t,g}(\nabla\vec{u}_g + (\nabla\vec{u}_g)^T):\nabla\vec{u}_g \quad (4)$$

$$C_\mu = 0.09,\ C_{1\varepsilon} = 1.44,\ C_{2\varepsilon} = 1.92,\ \sigma_k = 1,\ \sigma_\varepsilon = 1.3 \quad (5)$$

In this study, only one gas phase is modeled to represent all species including reactants, intermediate products, and products involved in STR within fluidized bed pyrolysis. Standard k-epsilon turbulent model and standard wall function submodels are used to describe the turbulence conditions of gas phase. The evolution and balance of gas species are modeled by using the PDF transport equation, see eq 6.

$$\frac{\partial\rho P}{\partial t} + \frac{\partial\rho u_i P}{\partial x_i} + \frac{\partial\rho S_k P}{\partial\psi_k} = -\frac{\partial}{\partial x_i}[\rho\langle u_i''|\psi\rangle P] + \frac{\partial}{\partial\psi_k}\left[\rho\left\langle\frac{1}{\rho}\frac{\partial J_{i,k}}{\partial x_i}|\psi\right\rangle P\right] \quad (6)$$

where ρ represents mean density of gas mixture; P is the Favre joint PDF of composition, u_i the Favre mean velocity vector of gas mixture, S_k the reaction rate for species k, ψ the composition space vector, u_i'' the velocity fluctuation vector of gas mixture, and $J_{i,k}$ the molecular diffusion flux vector. The notation $\langle\cdots\rangle$ represents expectations, and $\langle A|B\rangle$ is the probability of event A conditional on event B occurring. PDF, denoted by P, symbolizes the fraction of the time that the gas mixture spends at each species, temperature, and pressure state. P has $N + 2$ dimensions, which includes the N species, temperature, and pressure spaces. Based on the PDF, any single-point thermo-chemical moment (e.g., mean temperature, mean reaction rate) can be computed. The advantage of the PDF transport method is that the highly nonlinear reaction term is completely closed and involves no modeling. The two terms on the right-hand side are the PDF change owing to scalar convection by turbulence (turbulent scalar flux) and molecular mixing and diffusion, respectively. The turbulent scalar flux term is modeled based on the gradient-diffusion hypothesis as

DOI: 10.1021/acs.iecr.5b02164
Ind. Eng. Chem. Res. 2015, 54, 8344−8355

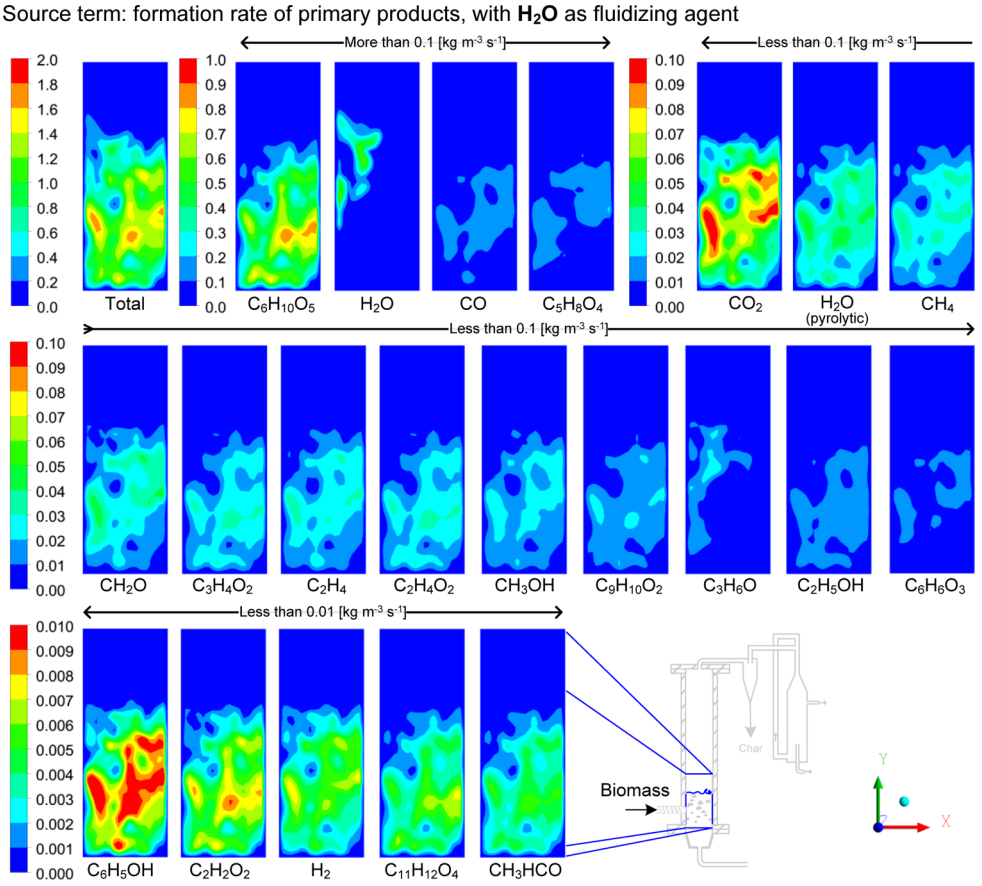

Figure 6. Instantaneous formation rate of individual primary products, implemented from the 3-D results from Mellin et al.,[2] with steam as fluidizing agent. Note that formed H_2O includes evaporated moisture and pyrolytic water (symbolized as H_2O (pyrolytic)).

Table 3. Proportion of Species Introduced by Source Terms into the Bed Zone, from Figures 5 and 6

	species									
atmosphere	CH_3OH	CH_4	$C_6H_{10}O_5$	H_2	H_2O	CH_3HCO	CO_2	CO	C_2H_5OH	C_2H_4
H_2O	1.79	2.34	46.65	0.45	11.08	0.35	6.15	9.81	0.01	2.12
N_2	1.64	2.19	44.36	0.42	12.87	0.33	5.68	9.19	0.79	1.98
continued	CH_2O	$C_2H_2O_2$	$C_2H_4O_2$	$C_{11}H_{12}O_4$	$C_5H_8O_4$	$C_9H_{10}O_2$	$C_6H_6O_3$	C_6H_5OH	$C_3H_4O_2$	C_3H_6O
H_2O	2.57	0.53	2.09	0.39	10.06	1.43	1.15	0.01	0.01	1.01
N_2	2.37	0.51	2.02	0.33	9.11	1.36	1.12	0.68	2.02	1.02

$$-\frac{\partial}{\partial x_i}[\rho\langle u_i''|\psi\rangle P] = \frac{\partial}{\partial x_i}\left(\frac{\rho\mu_t}{Sc_t}\frac{\partial P}{\partial x_i}\right) \quad (7)$$

where μ_t represents turbulent viscosity and Sc_t represents the turbulent Schmidt number. The $N + 1$ dimensional PDF transport equation is solved by a stochastic Monte Carlo approach because it is appropriate for high-dimensional equations. The Monte Carlo algorithm involves notional particles that move randomly through physical space owing to particle convection and also through composition space owing to molecular mixing and reaction. Molecular diffusion is modeled using the modified curl model.[22,23] The particle composition vector $\psi = (Y_1, Y_2, ..., Y_N, T, P)$ of each notional particle in the Monte Carlo method reaction is updated at each particle reaction fraction step Δt as

$$\psi^1 = \psi^0 + \int_0^{\Delta t} S\,dt \quad (8)$$

where Y_k is the kth species mass fraction, T the temperature, and P the pressure. S is the chemical source term.

2.2.3. Transfer of Primary Products to Secondary Pyrolysis Model. The geometry of the two models match, but the cell locations of the 3-D cross section do not match the 2-D mesh; hence, a transfer procedure was developed. Matlab 2014b was used to take the source term profiles of different primary compounds and adapt the field to the different cell locations of the 2-D mesh. More specifically, the *scatteredInterpolant* routine, employing linear interpolation and extrapolation, was used. The resulting formation rate profiles are shown in Figures 5 and 6; these are for nitrogen and steam as fluidizing agents from Mellin et al.,[2] respectively.

The total formation rate is given in Table 3; there is very slight difference in formation rate along the horizontal axis (X) between the cases, which is mostly due to instantaneous results being used. This also serves as an additional investigated factor in the parametric study. However, an important fact is that the formation rate is higher at the top of the bed when nitrogen is

DOI: 10.1021/acs.iecr.5b02164
Ind. Eng. Chem. Res. 2015, 54, 8344−8355

used a fluidizing agent. Figure 7 shows the total source, given as a cloud of points each representing a cell value, along the

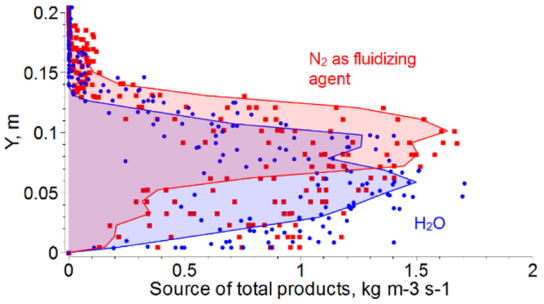

Figure 7. Formation rate along the height of the bed zone. Each dot represents one cell value, and a profile is shown along a pathline passing through the most formation-intense zone.

vertical axis, *Y*. The distribution is clearly different; a streamline (with shaded area under) through a slightly off-center path is shown as an example of the difference in profile.

2.2.4. Solution Strategy and Post Processing. In the bed zone, a fixed temperature is used which avoids the problem of mass forming with an uncontrollable reference temperature. Post processing was simplified by CFD-Post v 14.5; calculations to obtain molar fraction of compounds and calculating fractions presented in graphs were useful for analyzing the results. To explore the effect of reaction atmosphere, a parametric study was set up. Table 4 shows the parametric cases which were used; the same inlet gas velocity (and hence the same molar flow) were used.

To reflect the drop of pressure in the scrubber where the vapors are rapidly condensed, an outlet-pressure condition was applied to the outlet of −1 kPa.

Table 4. Cases in the Parametric Study of Temperature and Reaction Atmosphere

				temperature (°C)	
case no.	reaction atmosphere	Pp formation rate profile[a]	Mass flow relative to H_2O (wt %)	bed and reactor wall	cyclone and scrubber line
1	N_2	N_2	156	600	350
2	N_2	H_2O	156	~486.5[b]	250
3				600	350
4				650	400
5				700	450
6				800	450
7	H_2O	H_2O	100	~486.5[b]	250
8				600	350
9				650	400
10				700	450
11				800	450
12	CO	H_2O	155	600	350
13	CO_2	H_2O	244	600	350
14	H_2	H_2O	11	600	350
15	H_2O[c]	H_2O	100	600	350

[a]See Table 3 for primary product (Pp) formation rate profile. [b]In this case the fixed temperature field has some spatially variation because it is transferred from the primary pyrolysis simulation. [c]High-turbulence case with an inlet turbulent kinetic energy of 2850 m^2/s^2

3. RESULTS AND DISCUSSION

In this section, the results of the cases shown in Table 4 are analyzed and interpreted. A quantitative comparison with experimental results is first given; then, a study of temperature and reaction atmosphere influences on the prediction is presented.

3.1. Comparison with Experiments. At low temperatures (i.e., < 600 °C), the reaction atmosphere showed a limited influence on the overall vapor composition. In the experiment, reported in Kantarelis et al.,[24] a temperature of about 500 °C was used. In the modeling study,[2] by which the formation rate profiles where obtained, bed temperature (the gas in-bed temperature) was about 486.5 °C. However, for the comparison the case of 600 °C (see Table 4) was used for reasons discussed in section 3.3.

The trend of Figure 8 gives the lumped components of gas, water, and organic liquids in addition to the yield of gaseous species. To compare with the experimental results in the best possible way, the same solid residue yield is used and only the vapor components are compared. The wet basis is first used to check the overall agreement of lumped gas and liquid products. The dry basis is also presented, which shows a consistency in trend between experiment and model. Most importantly, we have noted a higher yield increase in gas (experiment, + 1.7 wt %; model, + 2.3 wt %) compared to organic liquid (experiment, + 0.8 wt %; model, + 0.2 wt %) when steam is added (and char yield thus reduced). Note that the dry basis excludes not only added steam and evaporated moisture but also pyrolytic water.

We can see that there is still a problem of insufficient water formation in the prediction of the new proposed model. This was also the case in our previous investigation[1] when using only the primary pyrolysis model. Some formation of water is expected in the condensation and aging of the liquid; however, such large amounts are unlikely to form. Instead, the kinetic model is likely in need of improvement.

In general, considering the overall distribution of products in the model against experiments, we have reason to conclude that this a fairly satisfactory prediction in terms of trend and absolute numbers. The kinetic scheme is calibrated toward a noncatalytic inert environment; however, because the scheme contains small individual reversible steps of the decomposition, the reaction atmosphere can for example suppress reactions with atmosphere component as a product. Physical aspects of the process, such as heat transfer and turbulence, are likely represented by the model fairly well. As such these considerations also take part, and while the effect of one atmosphere might be hard to trace back to one specific property, the atmosphere should influence the pyrolysis oil in the correct direction.

In Figure 9, the cracking severity is shown (molar ratio of CH_4 to the sum of C2s and C3s) depending on temperature and reaction atmosphere. Both experimental results and numerical predictions are shown. The temperature has a significant effect, but the reaction atmosphere also has a significant effect. The model correctly predicts high cracking severity in the case of a nitrogen atmosphere (compared to steam). However, this result is not observed at the temperature corresponding to the experiments. In fact, as shown below, a higher temperature was needed to have a reasonable extent of secondary pyrolysis. A temperature of ~500 °C resulted in no reactions at all.

DOI: 10.1021/acs.iecr.5b02164
Ind. Eng. Chem. Res. 2015, 54, 8344−8355

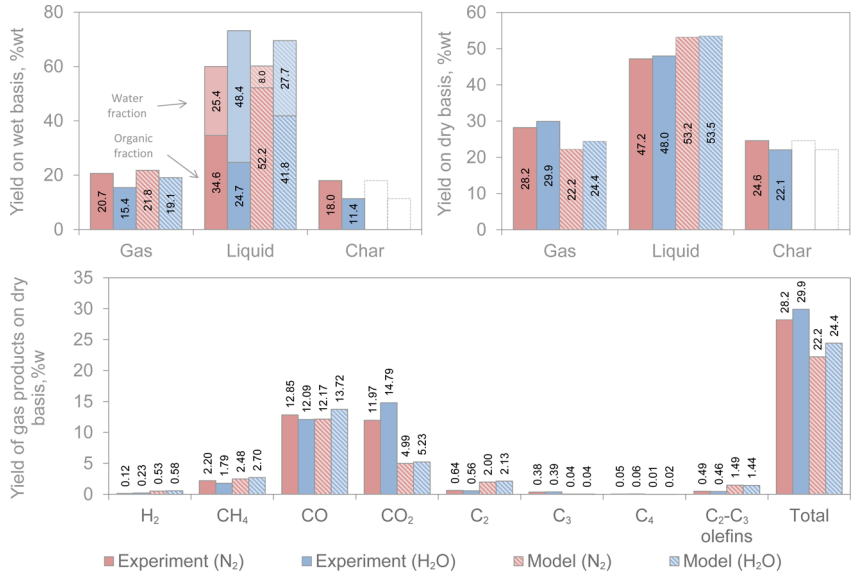

Figure 8. Distribution of pyrolysis products, (top left) showing products on wet basis and (top right) displaying products on dry basis (excluding input steam, evaporated moisture and pyrolytic water). Lower panel is the yield of gas products with hydrocarbons lumped. Model cases are at 600 °C; experiments[24] are at 500 °C.

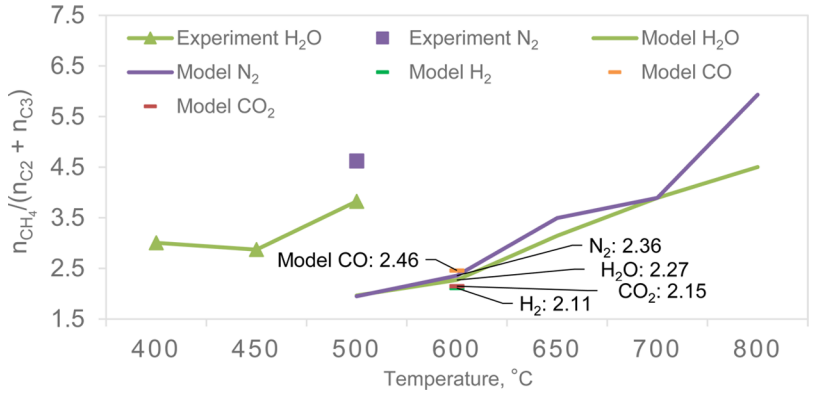

Figure 9. Cracking, indicated by molar ratio of CH_4 to the sum of C2s and C3s.

By comparing cases 1 and 3 in Table 4, no significant effects where found of primary products forming lower in the bed (when using steam), as shown in Figure 7.

3.2. Influence of Reaction Atmosphere N_2, H_2O, H_2, CO, and CO_2. The reaction atmosphere is first given in Figure 10, which shows the overall product yield (e.g., organic liquid and H_2O) and noncondensable gases at the outlet. As secondary pyrolysis reactions occur, the gas composition of primary pyrolysis with the inflow of fluidizing gas was eliminated from the outlet composition. In every case, the fluidizing atmosphere suppressed the release of each corresponding molecule.

The effect of the reaction atmosphere in the numerical predictions shows several interesting features. First, in Figure 11a, the effect on the outlet temperature is investigated. Here, as *x*-axis variable, heat capacity of the whole gas phase (mass-weighted average) is shown. There is strong correlation in that a less dense fluidizing gas will not bring the total heat capacity down as much. Hence, the temperature will be lower for the whole mixture. The same correlation persists (see Figure 11b) when the molecular weight of the fluidizing gas is used as the *x*-axis variable.

In Figure 11c, the total pressure drop divided by density (mass-weighted average), is given as the *x*-axis variable. The effect on residence time is shown, demonstrating a strong correlation. The gas accelerates when the whole vapor mixture has a low density. In turn, peak turbulent intensity increases as density decreases because of a higher velocity, which is shown in Figure 11d.

Low density of the whole vapor mixture reduces the residence time and also the outlet temperature, which can be seen in Figure 11a–c. This will intuitively result in a higher yield of condensable vapors; however, as seen in Figure 12, the opposite is actually predicted by the model. Here, the turbulence and chemistry interaction plays a bigger role. This can be seen in the case in which H_2O is used: alongside a high turbulence case, see H_2O (high turbulence).

For the case of H_2, the turbulent intensity is high and the reactivity of the atmosphere is also high, resulting in a reduction in the yield of condensable vapors. This is an interesting outcome of the simulation not consistent with studies such as Zhang et al.[25] in which a range of atmospheres were compared. Note that in ref 25 the results reflect the whole process using the corresponding atmosphere, including primary pyrolysis, secondary pyrolysis, quenching, and condensation.

DOI: 10.1021/acs.iecr.5b02164
Ind. Eng. Chem. Res. 2015, 54, 8344–8355

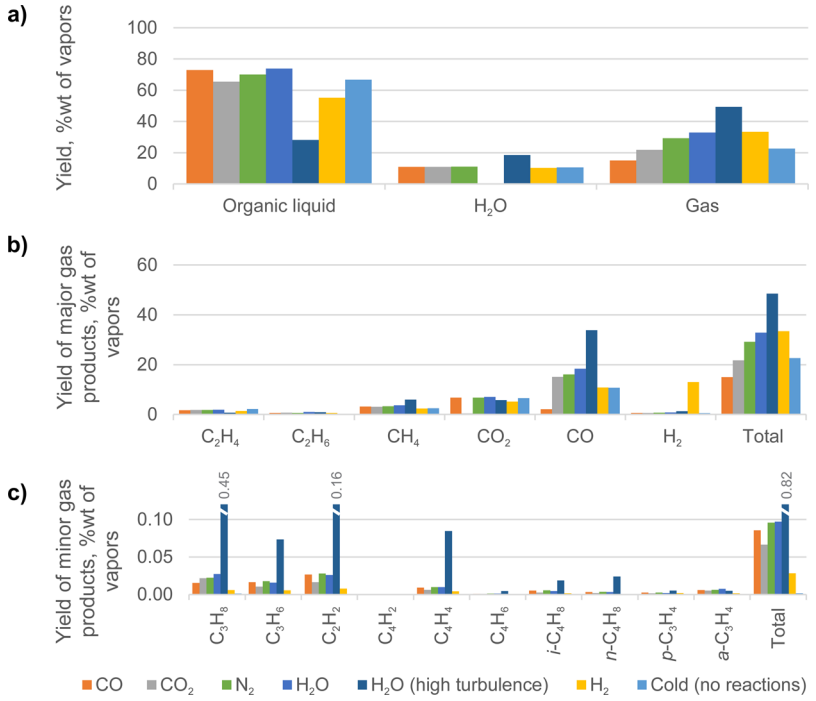

Figure 10. Effect of fluidizing gas on (a) overall yields and yields of noncondensable gases (b) showing major compounds and (c) minor compounds.

On the other hand, as observed and discussed by Xiong et al.,[26] the linkage between fluidizing gas velocity (thus residence time) and liquid yield is not monotonic. The reason is not clear, and high velocities might cause decomposition. Another reason could be the dynamics in the bed, which at high velocities will enter a different fluidization regime. Biomass particles can also be entrained before they have fully reacted; if they enter a region with lower heat-transfer capabilities, the char and gas yield will increase.

Nevertheless, the simulations using the atmospheres of lower reactivity suggest that there are significant physical effects that may affect the process, i.e., residence time and temperature. A complex set of factors is at play, and further analysis of the results could lead to greater understanding. However, uncertainty regarding the model should still be highlighted. Further testing and development of the kinetic scheme should be made, as was also called for by Norinaga et al.[13] Finally, more experimental conditions should be compared with model results.

As seen in Figure 12, the yield is highest in a H_2O atmosphere, but not because of low temperature and short residence time. Instead, according to the model, the low turbulent intensity is the reason for the high yield.

3.3. Influence of Temperature under H_2O and N_2 Atmosphere. In the cases indicated as ~486.5 °C, the fixed temperature field (varies slightly spatially) is transferred from the primary pyrolysis simulation, where the in-bed gas temperature is used. This gives the most consistent treatment; however, the kinetic scheme barely responds at all at this temperature. Hence, no decomposition occurs. Instead, the higher temperatures are used to give more reasonable results and for the study of reaction atmosphere.

As such, the temperature is important for the behavior of the comprehensive chemistry scheme. In fact, a temperature exceeding 627 °C (900 K) (at a residence time of 0.1s) was found to be necessary to observe the commonly found drop in oil yield.[16] At a residence time of 3 s, 527 °C (800 K) was found to give the same drop, which is similar to the residence time in our case. In Calonaci et al.,[16] a numerical residence time of about 5 s was used to obtain a typical decomposition of fast pyrolysis. In this numerical study, the residence time is dependent on the temperature because an equal molar flow rate was used in all cases (corresponding to an inlet velocity of 0.25 m/s at 500 °C).

In our simulation, 600 °C (873 K) was found to give reasonable results; as such, this case was used to compare with the experimental data. However, if the presence of catalytically active surfaces such as char, walls, and ash would be considered in the model, a similar yield drop at lower temperatures might occur.

As seen in Table 4, a wide temperature study was made for both N_2 and H_2O. Figure 13a shows the yield from the primary pyrolysis vapors on weight basis. Also shown is the effect on the outlet gas temperature (Figure 13b) and the residence time (Figure 13c). At high temperature, almost all the condensable compounds are gasified; however, in a conventional gasification process, a higher temperature is required to also gasify the char.

In Figure 14, at high temperatures the total yield increases alongside H_2, CH_4, CO, and C2s (including C_2H_2, C_2H_4, and C_2H_6). The other components have a weaker dependence on temperature. As seen in Figure 9, the cracking severity increases with temperature, meaning that CH_4 increases at the expense of higher hydrocarbons, which is also visible in Figure 14.

Using H_2O results in a higher CO content, at intermediate temperatures, compared to using N_2. This discrepancy accounts for almost the entire change in total yield, as all the other components remain fairly unaffected by the atmosphere. Although further analysis is needed, the reason might be that deoxygenation of condensable gas occurs because of decarbonylation instead of dehydration. In fact, the yield of water is much lower using a steam atmosphere (see Figure 10). As such, some water reacts, but the dehydration is also suppressed.

DOI: 10.1021/acs.iecr.5b02164
Ind. Eng. Chem. Res. 2015, 54, 8344−8355

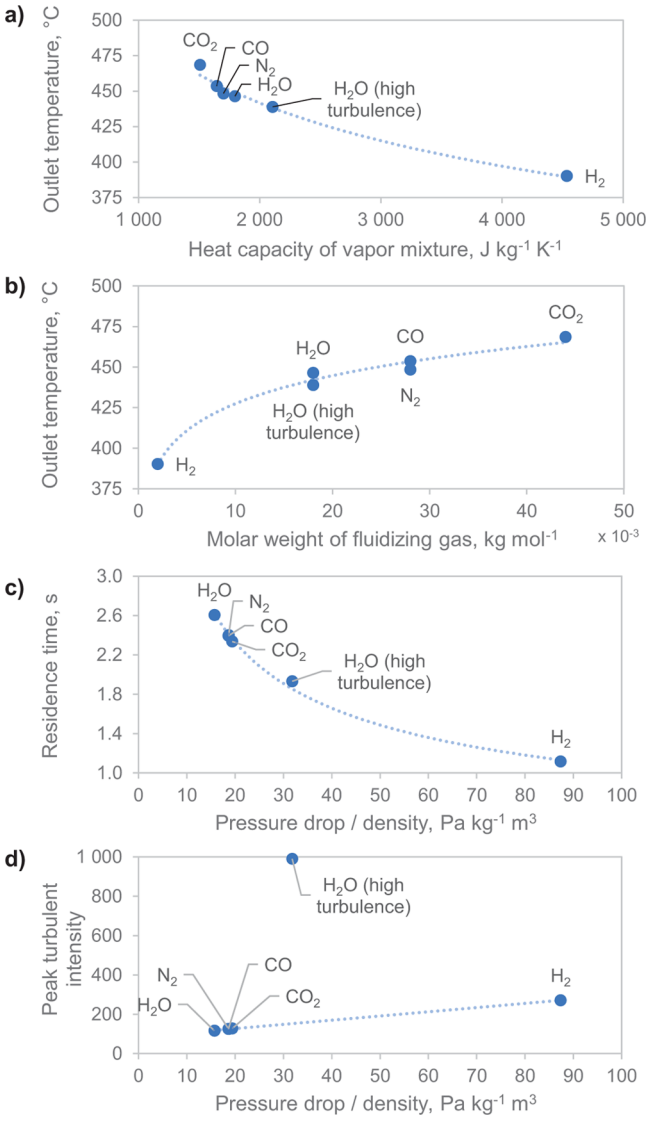

Figure 11. Effect of properties of the fluidizing atmospheres on the (a) outlet temperature, (b) outlet temperature, (c) residence time, and (d) peak turbulent intensity.

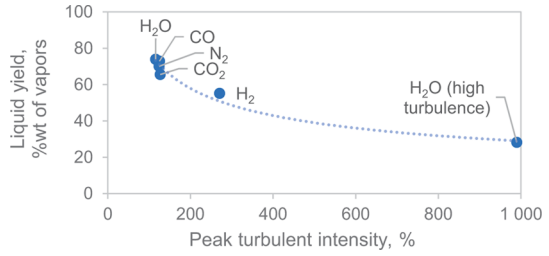

Figure 12. Effect of peak turbulent intensity for different reaction atmosphere on the yield of dry condensable liquid.

3.4. Radical Concentration. The radical behavior during pyrolysis is an interesting aspect that is possible to investigate with the aid of the model. It is not possible to model the polymerization (which also occurs in the liquid phase) with the aid of this kinetic scheme, but with the aid of the radical concentration, one can see the cause. Figure 15 shows the peak radical concentration depending on the reaction atmosphere. It indicates that the decomposition which occurs at high

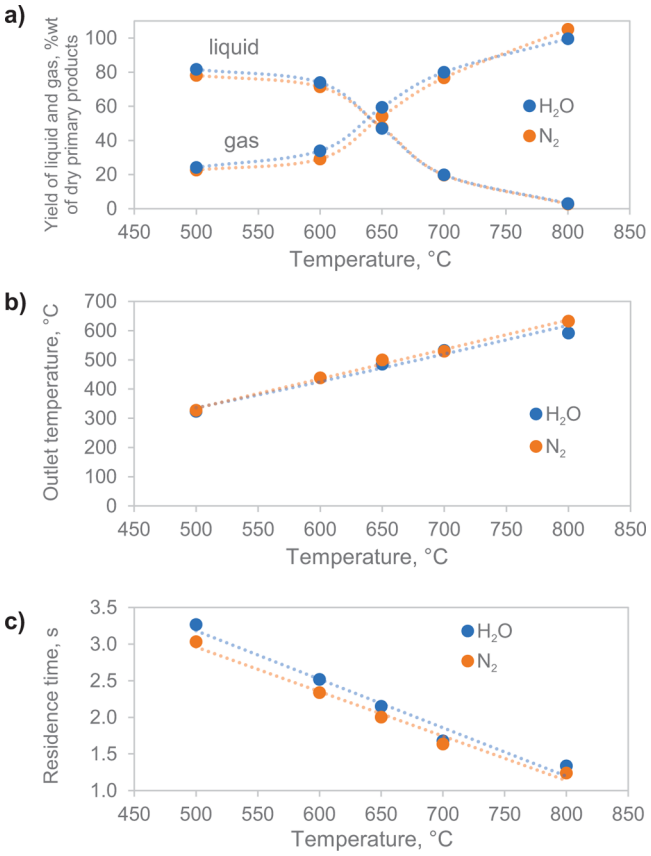

Figure 13. Effect of temperature on (a) the yield of gas and liquid, (b) the outlet temperature, and (c) the residence time.

turbulence (also at high temperatures) generates plenty of radicals. In the case of H_2O, at a normal degree of turbulence, an elevated amount of radicals compared to other atmospheres are generated. H_2 clearly generates the lowest total amount, though highly reactive atomic H radicals are formed.

According to Dutta et al.,[27] radical stabilization by water-hydrogen exchange seems to have a pronounced effect in bitumen cracking with steam. Figure 15 shows for each reaction atmosphere and temperature, the level of radicals in mole fraction. The case with steam shows a higher amount of radicals, even though the radical concentration is much lower than in, for example, combustion. Compare, for example, the highest case of H_2O, with a peak HO and HO_2 mole fraction of 7×10^{-12} and 8×10^{-11}, to a low-temperature (600 K) oxidation measurement[28] where HO and HO_2 mole fractions were approximated to 1×10^{-6} and 5×10^{-9}, respectively.

4. CONCLUSIONS

It is possible to implement the secondary pyrolysis scheme in a CFD framework, and simulations can be carried out in a time-effective manner. This is the first time such an effort has been made. The polymerization caused by radicals cannot be modeled; however, the concentration can be indicated. With aid of this model, the radicals have been studied at different reaction atmospheres and show a wide range of constituents. The radicals normally encountered in combustion are in this simulation low in concentration. Instead, radicals from the decomposition have been found in larger numbers.

To make the model respond correctly, an increase in temperature was needed, which is consistent with findings from

DOI: 10.1021/acs.iecr.5b02164
Ind. Eng. Chem. Res. 2015, 54, 8344−8355

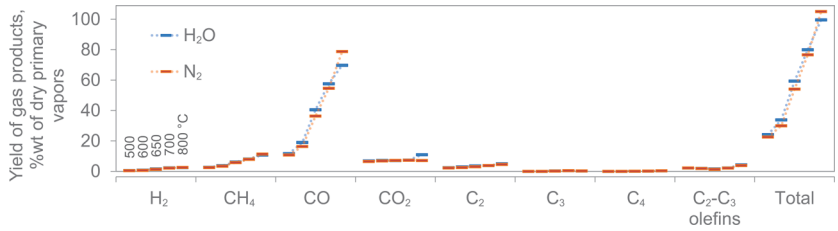

Figure 14. Effect of temperature (500−800 °C), when using H_2O and N_2 as fluidizing agent, on the yield of gas products from primary vapors.

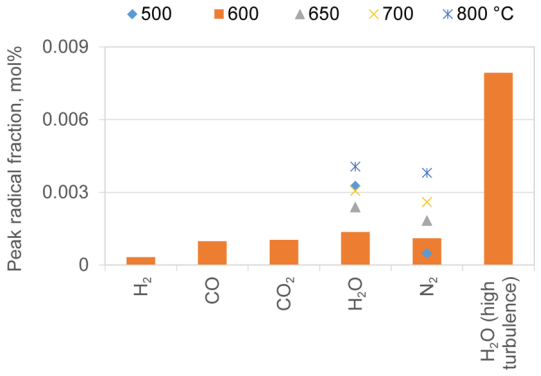

Figure 15. Peak radical concentration, depending on reaction atmosphere, temperature, and for one case, high turbulence.

previous contributions. The model temperature at 600 °C was chosen for the comparison versus experiments at 500 °C.

Within the framework of the model, the effects of H_2, CO, CO_2, H_2O, and N_2 were considerable, both in a physical and chemical sense. Each atmosphere except H_2 suppressed the release of each corresponding molecule during secondary pyrolysis. Residence time was affected by the atmosphere, from a minimum of 1.2 s (using H_2) to a maximum of 2.6 s (using H_2O).

As such, H_2O resulted in the longest residence time but also the highest liquid yield at the outlet. This appears to be due to low turbulence. A repeated case using high turbulence at the inlet resulted in extensive destruction of tar.

A H_2 atmosphere proved to be the most extreme case in the other direction, producing a low liquid yield due to higher turbulence. This case also resulted in the biggest deviation from commonly known trends; thus, the model cannot be considered completely reliable. The total radical concentration was overall lower (although atomic H radicals were high in concentration), and decomposition of higher hydrocarbons occurred, which gave high hydrogen content in the gas. Suppression of H_2 release might still occur, but it was counteracted by the above named mechanisms to give a hydrogen yield higher than that of the other atmospheres.

AUTHOR INFORMATION

Corresponding Authors

*E-mail: pmellin@kth.se.

*E-mail: x.yu3@aston.ac.uk.

Notes

The authors declare no competing financial interest.

ACKNOWLEDGMENTS

The authors gratefully acknowledge the Swedish Energy Agency (Energimyndigheten) for financial support of the research work (Project 33284-1). KIC Innoenergy is also acknowledged for the possibility of making this a collaborative work between KTH Royal Institute of Technology and Aston University.

REFERENCES

(1) Mellin, P.; Kantarelis, E.; Yang, W. Computational fluid dynamics modeling of biomass fast pyrolysis in a fluidized bed reactor, using a comprehensive chemistry scheme. *Fuel* **2014**, *117*, 704−715.

(2) Mellin, P.; Kantarelis, E.; Zhou, C.; Yang, W. Simulation of Bed Dynamics and Primary Products from Fast Pyrolysis of Biomass: Steam Compared to Nitrogen as a Fluidizing Agent. *Ind. Eng. Chem. Res.* **2014**, *53*, 12129−12142.

(3) Mellin, P.; Zhang, Q.; Kantarelis, E.; Yang, E. An Euler-Euler Approach to Modeling Biomass Fast Pyrolysis in Fluidized-Bed Reactors − Focusing on the Gas Phase. *Appl. Therm. Eng.* **2013**, *58*, 344−353.

(4) Palla, V. S. K. K.; Papadikis, K.; Gu, S. Computational modelling of the condensation of fast pyrolysis vapours in a quenching column. Part A: Hydrodynamics, heat transfer and design optimization. *Fuel Process. Technol.* **2015**, *131*, 59−68.

(5) Morf, P.; Hasler, P.; Nussbaumer, T. Mechanisms and kinetics of homogeneous secondary reactions of tar from continuous pyrolysis of wood chips. *Fuel* **2002**, *81*, 843−853.

(6) Milne, T. A.; Abatzoglou, N.; Evans, R. J. *Biomass Gasifier "Tars": Their Nature, Formation and Conversion*; NREL/TP-570-25357; National Renewable Energy Laboratory: Golden, CO, 1999.

(7) Hoekstra, E.; Westerhof, R. J. M.; Brilman, W.; Van Swaaij, W. P. M.; Kersten, S. R. A.; Hogendoorn, K. J. A; Windt, M. Heterogeneous and homogeneous reactions of pyrolysis vapors from pine wood. *AIChE J.* **2012**, *58*, 2830−2842.

(8) Mellin, P.; Yang, W.; Yu, X. Comprehensive secondary pyrolysis in fluidized-bed fast pyrolysis of biomass, a fluid dynamics based modelling effort. *Energy Procedia* **2015**, *66*, 281−284.

(9) Wurzenberger, J. C.; Wallner, S.; Raupenstrauch, H.; Khinast, J. G. Thermal conversion of biomass: Comprehensive reactor and particle modeling. *AIChE J.* **2002**, *48*, 2398−2411.

(10) Boroson, M. L.; Howard, J. B.; Longwell, J. P.; Peters, W. A. Heterogeneous cracking of wood pyrolysis tars over fresh wood char surfaces. *Energy Fuels* **1989**, *3*, 735−740.

(11) Elfasakhany, A. Modeling of Secondary Reaction of Tar (SRT) using a Functional Group Model. *Int. J. Mech. Eng. Technol.* **2012**, *3*, 123−136.

(12) Ranzi, E.; Corbetta, M.; Manenti, F.; Pierucci, S. Kinetic modeling of the thermal degradation and combustion of biomass. *Chem. Eng. Sci.* **2014**, *110*, 2−12.

(13) Norinaga, K.; Shoji, T.; Kudo, S.; Hayashi, J.-i. Detailed chemical kinetic modelling of vapour-phase cracking of multi-component molecular mixtures derived from the fast pyrolysis of cellulose. *Fuel* **2013**, *103*, 141−150.

(14) Gilbert, P.; Ryu, C.; Sharifi, V.; Swithenbank, J. Tar reduction in pyrolysis vapours from biomass over a hot char bed. *Bioresour. Technol.* **2009**, *100*, 6045−6051.

(15) Ranzi, E.; Cuoci, A.; Faravelli, T.; Frassoldati, A.; Migliavacca, G.; Pierucci, S.; Sommariva, S. Chemical Kinetics of Biomass Pyrolysis. *Energy Fuels* **2008**, *22*, 4292−4300.

(16) Calonaci, M.; Grana, G.; Hemings, E. B.; Bozzano, G.; Dente, M.; Ranzi, E. Comprehensive Kinetic Modeling Study of Bio-oil

DOI: 10.1021/acs.iecr.5b02164
Ind. Eng. Chem. Res. 2015, 54, 8344−8355

Formation from Fast Pyrolysis of Biomass. *Energy Fuels* **2010**, *24*, 5727−5734.
(17) Pope, S. B. PDF methods for turbulent reactive flows. *Prog. Energy Combust. Sci.* **1985**, *11*, 119−192.
(18) Zhang, Y. L.; Luo, Y. H.; Wu, W. G.; Zhao, S. H.; Long, Y. F. Heterogeneous Cracking Reaction of Tar over Biomass Char, Using Naphthalene as Model Biomass Tar. *Energy Fuels* **2014**, *28*, 3129−3137.
(19) Wang, Y.; Yan, L. CFD Studies on Biomass Thermochemical Conversion. *Int. J. Mol. Sci.* **2008**, *9*, 1108−1130.
(20) Pope, S. B. Computationally efficient implementation of combustion chemistry using in situ adaptive tabulation. *Combust. Theory Modell.* **1997**, *1*, 41−63.
(21) Launder, B. E.; Spalding, D. B. *Lectures in Mathematical Models of Turbulence*; Academic Press: London, 1972.
(22) Janicka, J.; Kolbe, W.; Kollmann, W. Closure of the transport-equation for the probability density-function of turbulent scalar fields. *J. Non-Equilib. Thermodyn.* **1979**, *4*, 47−66.
(23) Nooren, P. A.; Wouters, H. A.; Peeters, T. W. J.; Roekaerts, D.; Maas, U.; Schmidt, D. Monte Carlo PDF modelling of a turbulent natural-gas diffusion flame. *Combust. Theory Modell.* **1997**, *1*, 79−96.
(24) Kantarelis, E.; Yang, W.; Blasiak, W. Production of liquid feedstock from biomass via steam pyrolysis in a fluidised bed reactor. *Energy Fuels* **2013**, *27*, 4748−4759.
(25) Zhang, H.; Xiao, R.; Wang, D.; He, G.; Shao, S.; Zhang, J.; Zhong, Z. Biomass fast pyrolysis in a fluidized bed reactor under N_2, CO_2, CO, CH_4 and H_2 atmospheres. *Bioresour. Technol.* **2011**, *102*, 4258−4264.
(26) Xiong, Q.; Aramideh, S.; Kong, S. C. Modeling Effects of Operating Conditions on Biomass Fast Pyrolysis in Bubbling Fluidized Bed Reactors. *Energy Fuels* **2013**, *27*, 5948−5956.
(27) Dutta, R. P.; McCaffrey, W. C.; Gray, M. R.; Muehlenbachs, K. Thermal Cracking of Athabasca Bitumen: Influence of Steam on Reaction Chemistry. *Energy Fuels* **2000**, *14*, 671−676.
(28) Blocquet, M.; Schoemaecker, C.; Amedro, D.; Herbinet, O.; Battin-Leclerc, F.; Fittschen, C. Quantification of OH and HO2 radicals during the low-temperature oxidation of hydrocarbons by Fluorescence Assay by Gas Expansion technique. *Proc. Natl. Acad. Sci. U. S. A.* **2013**, *110*, 20014−20017.

DOI: 10.1021/acs.iecr.5b02164
Ind. Eng. Chem. Res. 2015, 54, 8344−8355